Electrocatalysts

International Edition: DOI: 10.1002/anie.201506480
German Edition: DOI: 10.1002/ange.201506480

Metallic Co_4N Porous Nanowire Arrays Activated by Surface Oxidation as Electrocatalysts for the Oxygen Evolution Reaction

Pengzuo Chen, Kun Xu, Zhiwei Fang, Yun Tong, Junchi Wu, Xiuli Lu, Xu Peng, Hui Ding, Changzheng Wu, and Yi Xie*

Abstract: *Designing highly efficient electrocatalysts for oxygen evolution reaction (OER) plays a key role in the development of various renewable energy storage and conversion devices. In this work, we developed metallic Co_4N porous nanowire arrays directly grown on flexible substrates as highly active OER electrocatalysts for the first time. Benefiting from the collaborative advantages of metallic character, 1D porous nanowire arrays, and unique 3D electrode configuration, surface oxidation activated Co_4N porous nanowire arrays/carbon cloth achieved an extremely small overpotential of 257 mV at a current density of 10 mA cm^{-2}, and a low Tafel slope of 44 mV dec^{-1} in an alkaline medium, which is the best OER performance among reported Co-based electrocatalysts to date. Moreover, in-depth mechanistic investigations demonstrate the active phases are the metallic Co_4N core inside with a thin cobalt oxides/hydroxides shell during the OER process. Our finding introduces a new concept to explore the design of high-efficiency OER electrocatalysts.*

The continuous depletion of fossil fuels and rising environmental concerns are triggering considerable research interests in alternative energy storage and conversion systems.[1] The oxygen evolution reaction (OER), as one of the most significant processes in water splitting, has stimulated extensive studies in recent years.[2] However, the OER process usually suffers from multiple steps of proton-coupled electron transfer, leading to very sluggish kinetic reactions.[3] To date, the most efficient electrocatalysts for water oxidation reaction are precious metal oxides.[4] However, the high cost and scarcity of these noble metals severely limit their practical applications. Therefore, the development of highly efficient electrode materials with low overpotential and superior stability for OER is actively being pursued.

Over the past years, cobalt-based material systems[5] have been widely investigated as promising non-noble catalysts for water oxidation. However, most of those catalysts usually require grafting onto glassy carbon by using polymer binder (nafion or PTFE) in aqueous electrolytes. The whole process is time-consuming, and the catalytic activity of OER catalysts is significantly inhibited by the small catalytic surface area and inefficient mass diffusion of electrons.[6] Also, the stability of the electrocatalysts is greatly influenced during the whole OER process because of the continuous evolution of O_2 bubbles from the electrodes, resulting in the peeling of the coated electrocatalysts.[7] Thus, it is highly desirable to develop alternative electrode configurations with high electrocatalytic activity and superior long-term stability for OER.

Recently, well-defined one-dimensional (1D) nanowire arrays directly grown on the current collectors represent a new high-efficiency electrode configuration owing to the synergetic advantages of the faster electrolyte penetration and diffusion of ionic species, greater electrical conductivity, and higher structural stability.[8] Most of the reports on the utilization of nanowire arrays for OER are focused on semiconducting cobalt oxide nanowires.[9] Unfortunately, the intrinsically inferior electrical conductivity of these semiconducting Co-based electrocatalysts would significantly hamper the electron transfer between the nanowires arrays and the current collector interfaces, limiting their overall OER efficiency. Thus, it is highly desirable to design metallic Co-based nanowire arrays directly grown on the current collector for OER.

Density functional theory suggests that Co_4N, as a metallic Co-based material, could provide an ideal platform for investigations of the OER catalytic activity of metallic Co-based compounds.[10] Density functional theory (DFT) calculation reveals that the density of states (DOS) across the Fermi level, demonstrating the metallic character of the Co_4N (Figure 1). The typical metallic behavior of Co_4N can be further revealed by the temperature-dependent electrical resistance curve (Figure 1b), where electrical resistance increased approximately linearly with elevating temperature,

[*] P. Chen,[+] K. Xu,[+] Z. Fang, Y. Tong, J. Wu, X. Lu, X. Peng, H. Ding, Prof. C. Wu, Prof. Y. Xie
Hefei National Laboratory for Physical Science at the Microscale, iChEM (Collaborative Innovation Center of Chemistry for Energy Materials),
Hefei Science Center (CAS) and CAS Key Laboratory of Mechanical Behavior and Design of Materials,
University of Science & Technology of China
Hefei, Anhui 230026 (P.R. China)
E-mail: czwu@ustc.edu.cn

[+] These authors contributed equally to this work

Supporting information for this article is available on the WWW under http://dx.doi.org/10.1002/anie.201506480.

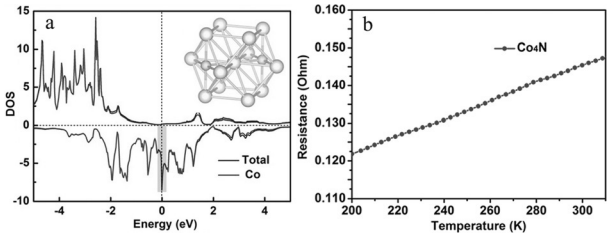

Figure 1. a) Calculated density of states (DOS) for Co_4N product. Inset: corresponding crystal structure of Co_4N product with dominant Co–Co metallic bonds. b) Temperature-dependent electrical resistance of Co_4N product.

consistent with a metallic character. In this regard, metallic Co_4N would bring efficient transfer of electrons between the catalyst surface and the current collector, showing potential application in the field of OER. Herein, we report the first metallic porous nanowire arrays grown on carbon cloth (denoted as Co_4N NW/CC). Benefiting from the intrinsic metallic character to favor the fast charge transport, 1D porous nanowire arrays for large active surface area, and 3D configuration structure for strong structure stability, metallic Co_4N NW/CC electrodes activated by surface oxidation not only show excellent OER catalytic performance with extremely small overpotential of 257 mV at a current density of 10 mA cm^{-2} and low Tafel slope of 44 mV dec^{-1}, but also exhibit excellent stability during a prolonged OER process in an alkaline medium.

The nitridation method has been proven to be an effective way to prepare specific cobalt nitrides.[11] In our case, metallic Co_4N porous nanowire arrays grown on carbon cloth are first synthesized by a simple nitridation reaction, with high temperature treatment of Co(OH)F nanowire arrays precursor under a flowing NH_3 atmosphere (Scheme 1; Supporting Information, Figure S3).[12] The overall reaction equation for the formation of Co_4N can be shown as following: $24\,Co(OH)F + 40\,NH_3 = 6\,Co_4N + 24\,H_2O + 5\,N_2 + 24\,NH_4F$. The structural information of the as-obtained samples were first investigated by X-ray diffraction (XRD). All diffraction peaks of the product match well with the pure Co_4N phase with a cubic structure, indicating that the Co(OH)F precursors was successfully converted into Co_4N product (Figure 2a). Meanwhile, the Co_3O_4 nanowires can also be prepared by oxidation reaction for further comparison (Supporting Information, Figures S4, S5). SEM and TEM images demonstrated that the 3D configuration based on porous Co_4N nanowire arrays had been developed successfully (Figure 2b,c; Supporting Information, Figure S6). Microscopic characterizations were also performed to further analyze the phases and compositions. The HRTEM image of Co_4N nanowires showed a distinct lattice fringe of 2.07 Å, which is consistent with the (111) lattice plane of Co_4N product (Figure 2d). Moreover, electron energy loss spectroscopy (EELS) confirmed that the resulting product was composed of Co and N, and EELS mapping images also confirmed the homogenous spatial distributions of Co and N in Co_4N product (Figure 2e,f).[13] Therefore, all the above results clearly suggested that the metallic Co_4N nanowires array was successfully obtained from the nitridation reaction of Co(OH)F NW precursor.

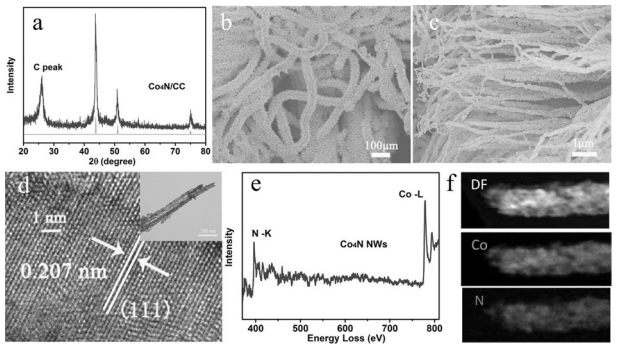

Figure 2. a) XRD pattern of Co_4N NW/CC. b) Low- and c) high-magnification SEM images of Co_4N NW/CC. d) HRTEM image of Co_4N NW/CC. Inset: TEM image of Co_4N NW/CC (scale bar = 200 nm). e) EELS spectra and f) the typical HAADF-STEM, EELS element mapping images of obtained Co_4N product.

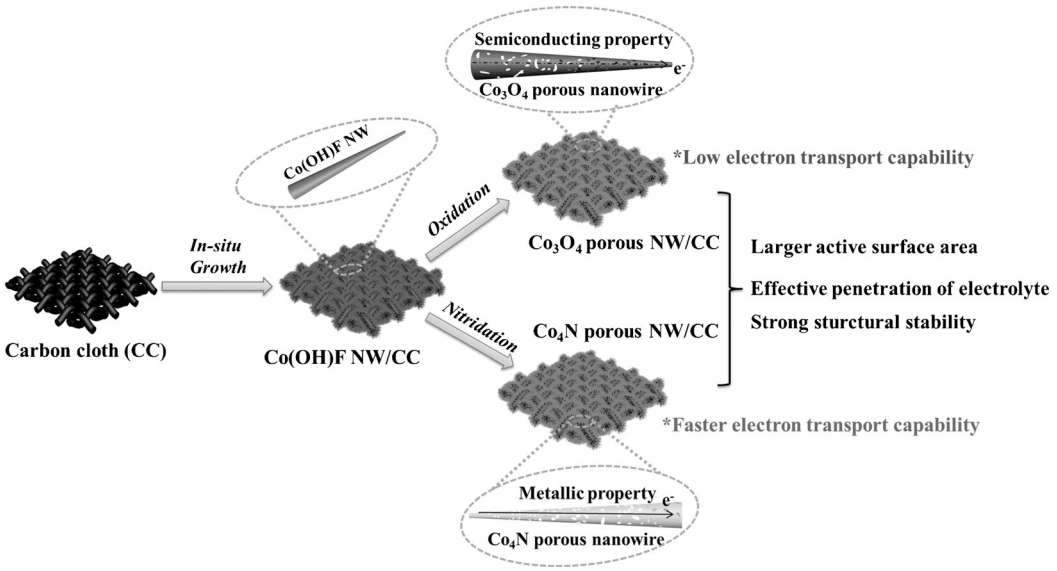

Scheme 1. Preparation process of Co(OH)F NW, Co_3O_4 NW, and Co_4N NW grown on carbon cloth.

To verify whether metallic Co_4N NW/CC could serve as a highly efficient OER electrocatalyst, electrochemical measurements were performed in 1M KOH solution. The Co_4N NW/CC electrode was firstly activated by surface oxidation in O_2-saturated alkaline medium for 20 cycles, and then recorded the twentieth cycle as the first polarization curves at a sweep rate of 5 mV s^{-1} (denoted surface oxidation activated Co_4N NW/CC as SOA-Co_4N NW/CC). The SOA-Co_4N NW/CC electrode displayed the smallest overpotential requirement of 257 mV to reach a current density of 10 mA cm^{-2}, while the Co(OH)F NW/CC precursor and Co_3O_4 NW/CC needed a relatively larger overpotential requirement of 375 mV and 320 mV, respectively (Figure 3a). This result suggested that the composition transformation of the Co(OH)F/CC to SOA-Co_4N/CC can significantly improve the catalytic activity. To gain further

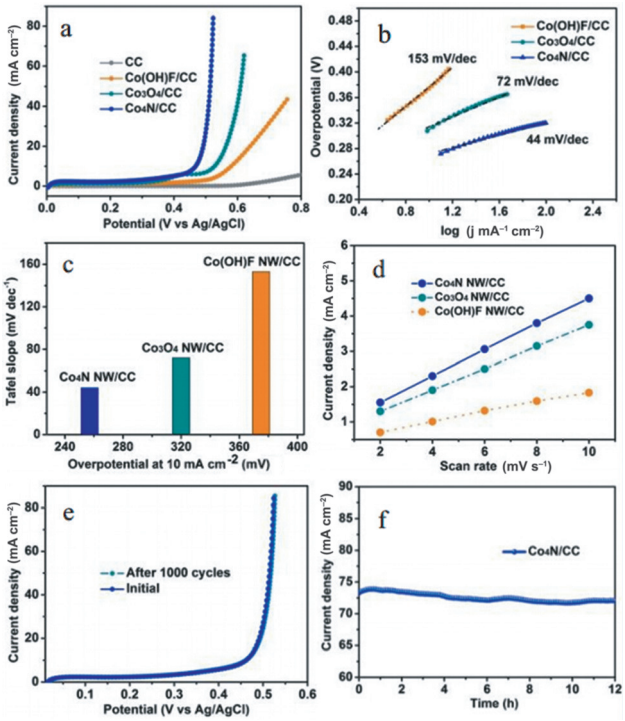

Figure 3. a) IR-corrected polarization curves, b) Tafel plots of all catalysts in 1 M KOH solution. c) Comparison of potentials required to reach $j = 10\ mA\,cm^{-2}$ and Tafel slopes for all as-obtained catalysts. d) Current density as a function of the scan rate for all as-obtained electrodes. e) IR-corrected polarization curves of SOA-Co_4N NW/CC before and after CV testing of 1000 cycles in 1 M KOH solution. f) Time dependence of the current density under a static overpotential of 320 mV in 1 M KOH solution.

insight into the SOA-Co_4N NW/CC electrode, the Tafel slopes for all catalysts were investigated. The Tafel slope of the SOA-Co_4N NW/CC electrode was 44 mV/dec, smaller than that of Co(OH)F NW/CC (153 mV/dec) and Co_3O_4 NW/CC (72 mV/dec; Figure 3b,c), indicating more rapid OER rates can be achieved in practical applications using SOA-Co_4N NW/CC as electrocatalyst (Supporting Information, Figure S7).

The porous nanowires arrays could provide a larger active surface area, which can be evaluated approximately by using the electrochemical double-layer capacitance (C_{dl}).[14] Porous SOA-Co_4N NW/CC ($365.5\ mF\,cm^{-2}$) exhibit a 1.2 and 2.6-times C_{dl} than Co_3O_4 NW/CC ($306.3\ mF\,cm^{-2}$) and Co(OH)F NW/CC ($141.2\ mF\,cm^{-2}$), respectively (Figure 3d; Supporting Information, Figure S8). Generally, the higher effective surface area contributed to the higher electrocatalytic activity of SOA-Co_4N nanowire arrays. However, the activity enhancement is not solely dependent on the increased electrochemical surface area. For example, the current density of SOA-Co_4N NW/CC electrode ($73.5\ mA\,cm^{-2}$) is approximately 7.4 times higher than that of Co_3O_4 NW/CC electrode ($10\ mA\,cm^{-2}$) at the overpotential of 320 mV (Figure 3a), which demonstrates the better charge transfer kinetics on metallic SOA-Co_4N nanowires. The above results clearly illustrate that the better catalytic performance of SOA-Co_4N NW/CC compared with Co_3O_4/CC and Co(OH)F/CC mainly originate from the N atoms incorporation and leads to a unique metallic electronic structure. Moreover, stability is another key index to evaluate the property of catalysts. The polarization curve achieved after 1000 cycles (Figure 3e; Supporting Information, Figure S9a) and chronoamperometric response (Figure 3f; Supporting Information, Figure S9b) all verify the high stability of SOA-Co_4N NW/CC, indicating the apparent advantage of metallic Co_4N porous nanowire arrays as high-performance OER electrocatalysts.

The superior OER catalytic performance of SOA-Co_4N NW/CC electrodes can be ascribed to the multiple synergistic effects of metallic character, 1D porous nanowire structure, and unique 3D electrode configuration. First, the metallic character of electrode material endows the faster charge transport capability between the catalyst surface and the current collector, favoring the high OER activity. Second, the porous SOA-Co_4N nanowire arrays provide a larger active surface area, which can be confirmed by the corresponding C_{dl} and BET surface areas (Supporting Information, Figure S14). Third, benefiting from the unique 3D electrode configuration, the reaction kinetics of oxygen evolution reaction can be significantly promoted. Also, one-dimensional (1D) nanowire direct grown on carbon cloth provides the straightway path for electron transport and enhances the structural stability, whilst well-defined porous nanowire arrays provide a smooth pathway to facilitate the penetration of electrolyte and augment the contact degree between reactants and active sites within Co_4N nanowires. Furthermore, 3D nanowire array structure also enable the facile release of evolved O_2 gas bubbles to further improve the reaction interface. Therefore, these collaborative advantages enable the porous SOA-Co_4N NW/CC to achieve excellent OER catalytic activity.

To better develop the metallic Co_4N as a highly active electrocatalyst, a deeper understanding of the catalytic mechanism is also needed. Generally, the possible OER catalytic mechanism of non-oxide Co-based catalysts has already been proposed in an alkaline medium.[15]

$$Co + 2\,OH^- \rightarrow Co(OH)_2 + 2\,e^- \quad (1)$$

$$3\,Co(OH)_2 + 2\,OH^- \rightarrow Co_3O_4 + 4\,H_2O + 2\,e^- \quad (2)$$

$$Co_3O_4 + H_2O + OH^- \rightarrow 3\,CoOOH + e^- \quad (3)$$

$$CoOOH + OH^- \rightarrow CoO_2 + H_2O + e^-$$
$$\text{Summary OER}: \ 4\,OH^- \rightarrow 2\,H_2O + O_2 + 4\,e^- \quad (4)$$

In our case, the catalytic mechanism of Co_4N is similar to that of the mechanism proposed above for Co-based catalysts during the OER process in an alkaline medium. Firstly, the Co atoms on the surface of Co_4N are partially surface oxidized into CoOOH to form the CoOOH/Co_4N as the active sites. These active sites can expedite the oxidation of absorbed OH^- species into molecular oxygen. Then, at higher potential, the CoOOH/Co_4N will be further oxidized to form the CoO_2/Co_4N complex species that is a more efficient species for OER process. Therefore, the active phases actually are metallic Co_4N cores with a thin cobalt oxide/hydroxide shell during water oxidation process,[16] The metallic Co_4N nanowire was selected mainly for its superior conductivity, which could

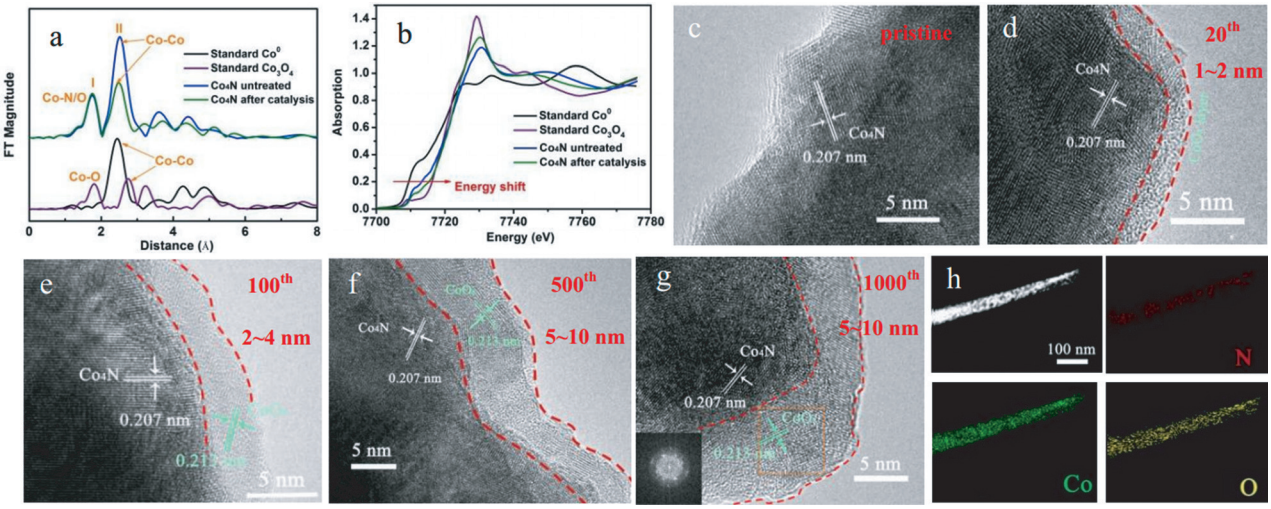

Figure 4. a) FT-EXAFS spectra and b) XANES profiles of standard Co, Co_3O_4, and Co_4N before and after 1000 potential cycles from 0-0.8 V. c) HRTEM image of pristine Co_4N sample (without activated) and HRTEM images after d) 20, e) 100, f) 500 and g) 1000 CV cycles. h) Corresponding element mapping images of Co_4N catalyst after 1000 potential cycling.

expedite electron transport from conductive support to the catalyst surface of metallic Co_4N porous nanowires much better than the semiconducting Co-based nanowires, guaranteeing a faster OER kinetics process compared with the semiconducting cores (Co_3O_4 and Co(OH)F) with very thin cobalt oxide/hydroxide shells as active sites.

To verify the catalytic mechanism, ex situ X-ray absorption fine structure (XAFS) spectroscopy has been performed. Figure 4a shows the Fourier transformed extended XAFS (FT-EXAFS) data for the Co_4N sample before and after potential cycling, compared with the standard Co foil and Co_3O_4. At first, it can be seen that the FT-EXAFS features, especially peak I at 1.8 Å corresponding to the Co–N/O bond, and peak II at 2.5 Å corresponding to the Co–Co bond, of the sample present a very basic similarity, demonstrating the elementary structure of the Co_4N layer remained stable during the OER process. The obvious difference of the both FT-EXAFS spectra is the "crashing decrease" of the FT intensity of the Co–Co shell and a small intensity increase of the first shell. The most possible interpret for this phenomenon is that the surface Co atoms of the layer have been oxidated. The Co_4N sample has a small alloying property with twelve Co coordinators, and the Co–Co distance is slightly longer than that of Co^0, but shorter than that of Co_3O_4, indicating the surface Co atoms of the layer have been partially oxidated into cobalt oxide/hydroxide, which is consistent with the result of XPS spectra (Supporting Information, Figure S15). However, XRD pattern (Supporting Information, Figure S16) still can't detect any cobalt oxides or other hydrated cobalt oxides, indicating a very thin cobalt oxide/hydroxide shell on the surface of Co_4N bulk. These systematic characterizations confirm that the major phase was Co_4N inside during OER process.

Moreover, the X-ray absorption near-edge spectra (XANES) of the Co_4N sample presents a pre-edge feature at about 7712 eV (Figure 4b). This feature became weaker after the potential cycling, suggesting the sample underwent a de-alloying process. On the other hand, the rising edge of the XANES shifts to higher energy gives further evidence for partial surface oxidation of the Co_4N sample. To investigate whether the active materials (CoO_x/Co_4N) is changing with the ongoing catalytic reaction process or not, we performed a list of ex situ HRTEM tests based on the Co_4N porous nanowires before (marked as pristine) and after cyclic voltammetry (CV) tests. As shown in Figure 4c, Co-O layer on pristine Co_4N sample could be hardly seen (below 1 nm owing to surface oxidation exposed to air). After 20 CV tests, a very thin CoO_x layer of 1–2 nm (4–9 CoO_x layers) was observed around the surface of Co_4N nanowires (Figure 4d), suggesting the electroactive species was formed on the Co_4N surface. Notably, the amount of electroactive species (CoO_x) was further increased and gradually reached the steady state with the prolonged CV tests (Figure 4e–g). This result reveals that the formation of CoO_x layer on the surface of Co_4N not only protects the Co_4N core from further oxidation, but also provides the necessary active sites for OER process. Meanwhile, the mapping images also show homogeneous oxygen element distribution around the whole Co_4N nanowires (Figure 4h). Moreover, the corresponding electrochemical measurements results reveal that the CoO_x layer formed on the surface of Co_4N nanowires plays a very important role for the OER. The catalytic activity of the Co_4N electrocatalyst becomes stable after 20 cycles, and no significant degradation was observed for the following CV cycles (Supporting Information. Figure S17). All of the above ex situ results provide solid evidence that the active phases are metallic Co_4N cores with a thin cobalt oxide/hydroxide shell during the OER process.

In conclusion, metallic Co_4N porous nanowire arrays were directly grown on a flexible substrate and were successfully derived by a facile precursor-nitridation reaction. Owing to their metallic property, 1D nanowire structure, and unique 3D electrode configuration, metallic Co_4N NW/CC electrodes activated by surface oxidation exhibit extremely high OER

catalytic activity, superior stability, and more favorable reaction kinetics. Furthermore, the catalytic mechanism of metallic Co_4N porous nanowires was shown to involve active phases that are metallic cobalt nitride cores with a thin cobalt oxide/hydroxide shell during the OER process. This work paves a new avenue to explore the design of advanced metallic catalysts.

Acknowledgements

The authors thank Prof. Xiaojun Wu at USTC for theoretical calculations to further understand the material property and Prof. Wangsheng Chu at USTC for the help of XAFS experiments and analyses. This work was financially supported by the National Basic Research Program of China (2015CB932302), the National Natural Science Foundation of China (21222101, U1432133, 11132009, 21331005, 11321503, U1532265, J1030412), the Chinese Academy of Sciences (XDB01020300), the Fok Ying-Tong Education Foundation, China (Grant No.141042), and the Fundamental Research Funds for the Central Universities (WK2060190027).

Keywords: 3D electrode configuration · cobalt nitride · electrocatalysts · oxygen evolution reaction · porous nanowire arrays

How to cite: *Angew. Chem. Int. Ed.* **2015**, *54*, 14710–14714
Angew. Chem. **2015**, *127*, 14923–14927

[1] a) M. D. Symes, L. Cronin, *Nat. Chem.* **2013**, *5*, 403–409; b) S. Chu, A. Majumdar, *Nature* **2012**, *488*, 294–303; c) T. R. Cook, D. K. Dogutan, S. Y. Reece, Y. Surendranath, T. S. Teets, D. G. Nocera, *Chem. Rev.* **2010**, *110*, 6474–6502.

[2] a) W. Zhou, X.-J. Wu, X. Cao, X. Huang, C. Tan, J. Tian, H. Liu, J. Wang, H. Zhang, *Energy Environ. Sci.* **2013**, *6*, 2921–2924; b) K. Xu, P. Chen, X. Li, Y. Tong, H. Ding, X. Wu, W. Chu, Z. Peng, C. Wu, Y. Xie, *J. Am. Chem. Soc.* **2015**, *137*, 4119–4125.

[3] a) J. Ren, M. Antonietti, T.-P. Fellinger, *Adv. Energy Mater.* **2015**, *5*, DOI: 10.1002/aenm.201401660.

[4] a) F. Li, B. Zhang, X. Li, Y. Jiang, L. Chen, Y. Li, L. Sun, *Angew. Chem. Int. Ed.* **2011**, *50*, 12276–12279; *Angew. Chem.* **2011**, *123*, 12484–12487; b) V. Petrykin, K. Macounova, O. A. Shlyakhtin, P. Krtil, *Angew. Chem. Int. Ed.* **2010**, *49*, 4813–4815; *Angew. Chem.* **2010**, *122*, 4923–4925.

[5] a) Y. Liu, H. Cheng, M. Lyu, S. Fan, Q. Liu, W. Zhang, Y. Zhi, C. Wang, C. Xiao, S. Wei, B. Ye, Y. Xie, *J. Am. Chem. Soc.* **2014**, *136*, 15670–15675; b) Y. Zhu, W. Zhou, Z.-G. Chen, Y. Chen, C. Su, M. O. Tadé, Z. Shao, *Angew. Chem. Int. Ed.* **2015**, *54*, 3897–3901; *Angew. Chem.* **2015**, *127*, 3969–3973; c) J.-I. Jung, H. Y. Jeong, J.-S. Lee, M. G. Kim, J. Cho, *Angew. Chem. Int. Ed.* **2014**, *53*, 4582–4586; *Angew. Chem.* **2014**, *126*, 4670–4674.

[6] V. Viswanathan, K. L. Pickrahn, A. C. Luntz, S. F. Bent, J. K. Nørskov, *Nano Lett.* **2014**, *14*, 5853–5857.

[7] J. Wang, H.-x. Zhong, Y.-l. Qin, X.-b. Zhang, *Angew. Chem. Int. Ed.* **2013**, *52*, 5248–5253; *Angew. Chem.* **2013**, *125*, 5356–5361.

[8] a) A.-L. Wang, X.-J. He, X.-F. Lu, H. Xu, Y.-X. Tong, G.-R. Li, *Angew. Chem. Int. Ed.* **2015**, *54*, 3669–3673; *Angew. Chem.* **2015**, *127*, 3740–3744; b) X. Xia, C. Zhu, J. Luo, Z. Zeng, C. Guan, C. F. Ng, H. Zhang, H. J. Fan, *Small* **2014**, *10*, 766–773.

[9] Y. Li, P. Hasin, Y. Wu, *Adv. Mater.* **2010**, *22*, 1926–1929.

[10] K. Oda, T. Yoshio, K. Oda, *J. Mater. Sci.* **1987**, *22*, 2729–2733.

[11] a) K. Zhang, L. Zhang, X. Chen, X. He, X. Wang, S. Dong, P. Han, C. Zhang, S. Wang, L. Gu, G. Cui, *J. Phys. Chem. C* **2013**, *117*, 858–865; b) Y. Cong, H. S. Park, H. X. Dang, F.-R. F. Fan, A. J. Bard, C. B. Mullins, *Chem. Mater.* **2012**, *24*, 579–586.

[12] a) J. Tian, Q. Liu, A. M. Asiri, X. Sun, *J. Am. Chem. Soc.* **2014**, *136*, 7587–7590; b) T. Chen, X. Li, C. Qiu, W. Zhu, H. Ma, S. Chen, O. Meng, *Biosens. Bioelectron.* **2014**, *53*, 200–206.

[13] N. Fontaíña-Troitiño, S. Liébana-Viñas, B. Rodríguez-González, Z.-A. Li, M. Spasova, M. Farle, V. Salgueiriño, *Nano Lett.* **2014**, *14*, 640–647.

[14] T. Y. Ma, S. Dai, M. Jaroniec, S. Z. Qiao, *J. Am. Chem. Soc.* **2014**, *136*, 13925–13931.

[15] N. H. Chou, P. N. Ross, A. T. Bell, T. D. Tilley, *ChemSusChem* **2011**, *4*, 1566–1569.

[16] N. Jiang, B. You, M. Sheng, Y. Sun, *Angew. Chem. Int. Ed.* **2015**, *54*, 6251–6254; *Angew. Chem.* **2015**, *127*, 6349–6352.

Received: July 14, 2015
Revised: August 28, 2015
Published online: October 6, 2015

